



Precipitation in eastern China over the past millennium varied with large-scale climate patterns

Mengyu Wang¹, Chaoyong Hu^{1,2}[✉], Yuhui Liu², Lianlian Li¹, Shucheng Xie² & Kathleen Johnson³

Modern precipitation variability over East China is known to be characterized by meridional tripole and dipole structures, linked to atmosphere and ocean dynamics. As the instrumental data may be influenced by anthropogenic global warming, it is unclear whether the physical mechanism underlying the tripole and dipole pattern have remained constant since the pre-industrial period. Here we investigate spatiotemporal precipitation variability over the past 1150 years using three high-resolution stalagmite $\delta^{18}\text{O}$ records from southern, central and northern China. Principal component analysis results suggest that the first principal component, reflecting large-scale Asian monsoon strength, is closely linked to solar variability. The second and third principal components, which reflect rainfall, reveal tripole and dipole patterns that persist over the last millennium and are driven by the Pacific Decadal Oscillation (PDO) and Atlantic Multidecadal Oscillation (AMO). We find that interactions between the monsoon, PDO, and AMO influence spatiotemporal rainfall patterns in East China.

¹School of Geography and Information Engineering, China University of Geosciences, Wuhan, China. ²State Key Laboratory of Biogeology and Environmental Geology, China University of Geosciences, Wuhan, China. ³Department of Earth System Science, University of California, Irvine, CA, USA. ✉email: chyhu@cug.edu.cn

Empirical orthogonal function (EOF) analysis of instrumental climate data indicates that the spatiotemporal pattern of rainfall variability in East China exhibits a tripole or a dipole structure^{1–8}. The tripole structure demonstrates a pattern of ‘-/+/-’ (rainfall decrease/increase/decrease) in South–Central–North China^{1,2,9}, while the dipole structure demonstrates a ‘+/-’ rainfall pattern from the south to the north of the Yangtze River^{5,10} (Fig. 1). These structures have been previously linked to the coupled ocean–atmosphere modes in the Pacific, including the El Niño southern oscillation (ENSO) and the Pacific decadal oscillation (PDO), and North Atlantic, including the North Atlantic oscillation (NAO) and Atlantic Multidecadal Oscillation (AMO), and their interaction with the East Asian monsoon^{3–5,8,11,12}. During the warm phase of ENSO

and PDO, there is a rainfall decrease in South and North China, but a rainfall increase around the Yangtze River area, showing a tripole pattern of ‘-/+/-’^{11,13}. The rainfall distribution pattern is also influenced by the North Atlantic, though, with a dipole pattern of ‘+/-’, with a rainfall increase in South China and a rainfall decrease in North China associated with a positive NAO and AMO^{5,14,15}. However, these patterns are based on meteorological data from recent decades, when the climate has been significantly influenced by human activities. Whether these patterns were the same before industrialization is still not well understood. Climate model simulations and paleoclimate reconstructions have suggested that similar rainfall patterns were found in East China during the little ice age (LIA), the medieval climate anomaly (MCA)^{16,17}, the Holocene¹⁸, and the last deglaciation¹⁹. However, due to the paucity of continuous high-resolution records, how the ocean–atmosphere coupling affects the spatial pattern of paleo-precipitation in East China is still unclear.

Chinese stalagmite oxygen isotope ($\delta^{18}\text{O}$) records with precise absolute chronology have revealed Asian monsoon variations from orbital to seasonal timescales^{20–29}. In recent years, with more published speleothem $\delta^{18}\text{O}$ records from different caves in East China, there is now potential to explore spatiotemporal climate variability in the region over longer timescales. However, Chinese speleothem $\delta^{18}\text{O}$ is influenced by multiple factors, such as moisture source region, precipitation amount, evaporation, etc., making the interpretation of speleothem $\delta^{18}\text{O}$ complicated. Some studies suggest that precipitation in the upstream areas is the main factor controlling stalagmite $\delta^{18}\text{O}$, which response to the variations of the Asian monsoon intensity^{27,30,31}. However, local precipitation and evaporation should not be ignored^{32–34}, as local rainfall amount and evaporation in the soil zone could also influence the $\delta^{18}\text{O}$ of rainfall and infiltrating cave water, thus modulating the stalagmite $\delta^{18}\text{O}$. Increased local and regional rainfall likely leads to a strong Rayleigh distillation and more negative $\delta^{18}\text{O}$ values, e.g., precipitation amount effect. At the same time, increased rainfall results in high relative humidity and weak evaporation, which also leads to more negative $\delta^{18}\text{O}$ values. That is, any single stalagmite $\delta^{18}\text{O}$ record likely contains both large-scale atmospheric circulation and local precipitation information, which are driven by complex ocean–atmosphere dynamics linked to the monsoon and coupled modes such as ENSO, PDO, NAO, and AMO. Separating these processes from spatially separated cave records could help to understand the ocean–atmosphere interaction over eastern China.

Principal component analysis (PCA) is a statistical procedure using orthogonal transformation to convert a set of observations of possibly correlated variables into a set of values of linearly uncorrelated variables, which could separate signals from different sources. For example, Chinese stalagmite oxygen isotope signals likely contain both Asian monsoon (isotopic fractionation by the variation of upper stream precipitation) and local rainfall amount (amount effect and evaporation) information. So, different cave locations in the monsoon area contain the common monsoon signal but different local rainfall amount information. That means that PCA of the different cave $\delta^{18}\text{O}$ records from eastern China should separate the monsoon and local rainfall signals, and the past spatial rainfall distribution pattern in the past could be reconstructed.

In this study, we present a continuous annually resolved $\delta^{18}\text{O}$ record spanning the past 1150 years (850–2000 CE) from Heshang Cave, Central China. Then combined with the published speleothem $\delta^{18}\text{O}$ records from Wanxiang Cave, Gansu²⁸, and Dongge Cave, Guizhou²⁹, we identify three principal components which are linked to monsoon and local rainfall distribution patterns. Finally, we investigate the influence of the Asian monsoon, PDO, and AMO on the spatiotemporal rainfall patterns in East

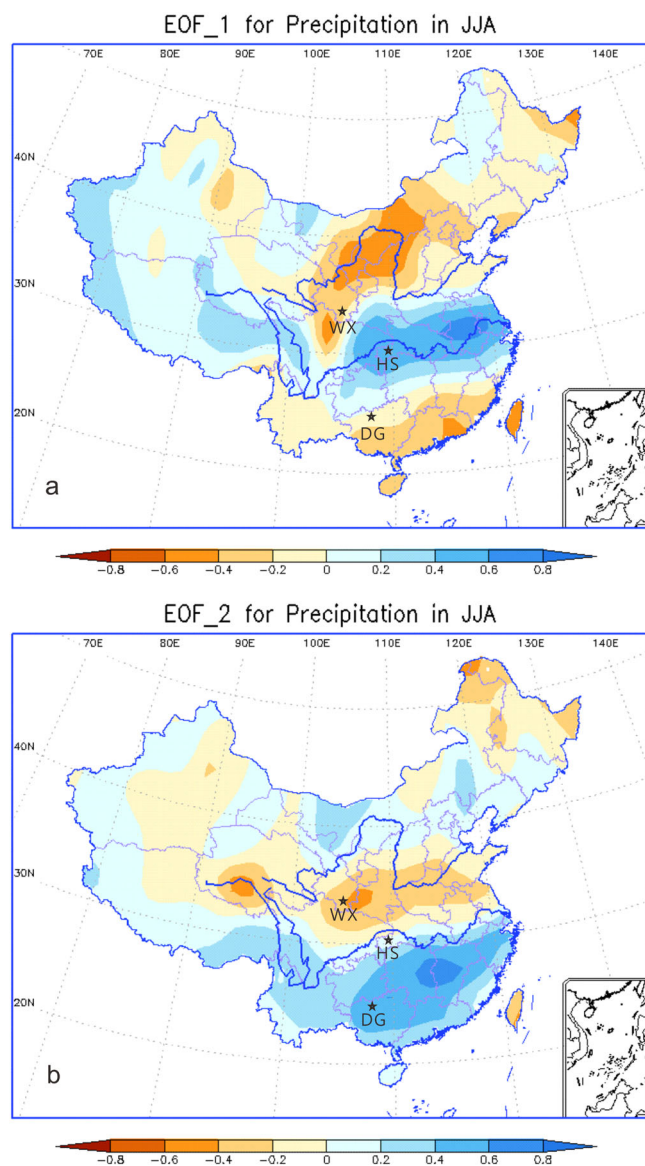


Fig. 1 The rainfall spatial distribution structures in eastern China from 1951 to 2012 CE. The tripole rainfall pattern presents anti-phased changes between central China and northern and southern China (a). The dipole rainfall pattern reflects the anti-phased change between southern and northern China (b). The stars mark the cave locations of Dongge²⁹, Heshang (this study), and Wanxiang²⁸, where three high-resolution stalagmite $\delta^{18}\text{O}$ records come from. We added the research sites on the base map from ref. ³⁵.

China over the last millennium. Dongge, Heshang, and Wanxiang caves are located in South, Central, and North China, respectively, and are ideally situated to test whether the modern rainfall tripole and dipole structures³⁵ existed in the past (Fig. 1).

Results

New annual resolution $\delta^{18}\text{O}$ record from Heshang cave, Central China. Early studies confirmed that distinguishable laminations in stalagmite HS4 are annual^{23,36,37}. By sampling along each lamina (Fig. 2), a continuous annual resolution $\delta^{18}\text{O}$ record covering 850–2000 CE is established (see Supplementary data 1). The variation of HS4 annual $\delta^{18}\text{O}$ record has been shown to be similar to other high-resolution speleothem records from nearby caves^{38,39} in recent centuries (Fig. 3), indicating it likely represents a robust record of regional $\delta^{18}\text{O}$ variation in Central China. Stalagmite DX1 and DX2, from Dongge cave, South China, are also annually laminated and an annual resolution $\delta^{18}\text{O}$ record is composited²⁹. Though the layers of the stalagmite from Wanxiang cave, North China, are not clear, the extra high concentrations of uranium with low ^{230}Th values provide a chronologic uncertainty of fewer than 2 years, and high-resolution sampling of stalagmite WX42B provides a $\delta^{18}\text{O}$ record with a resolution of 2.5 years²⁸. With these three precisely-dated high-resolution stalagmite $\delta^{18}\text{O}$ records covering the past 1150 years, we aim to investigate spatiotemporal rainfall patterns in East China during different climate stages over the last millennium, such as the current warm period (CWP), the LIA, and MCA.

Unlike the similar orbital-scale trends revealed from stalagmite $\delta^{18}\text{O}$ across the broad Asian monsoon region^{20,22,24,25}, the three highly-resolved stalagmite $\delta^{18}\text{O}$ records (Fig. 4) from Dongge, Heshang, and Wanxiang caves (DG, HS, and WX hereafter) show different variations over the last millennium. The differences likely indicate that though all the records are from eastern China and share a common Asian monsoon signal, the interannual to centennial-scale stalagmite $\delta^{18}\text{O}$ variability at each site is likely modulated by different local climate signals (e.g., precipitation and evaporation) and karst hydrologic processes^{32,33}. Wavelet analysis reveals distinct inter-annual, inter-decadal, and centennial cycles from the three stalagmites $\delta^{18}\text{O}$ records (Fig. 4) which may indicate the differing impacts of internal climate variability on rainfall at each site^{37,40–42}.

PCA of the spatially separated cave records. Here, we aim to separate the monsoon signal from these spatial precipitation patterns in East China through PCA analysis of the three $\delta^{18}\text{O}$ records (Fig. 5). The PC1 explains 42.28% of the variability. The loadings for DX, HS, and WX $\delta^{18}\text{O}$ are 0.69, 0.24, and 0.68, respectively, indicating a common signal is extracted from the three $\delta^{18}\text{O}$ records (Fig. 5a). As all Chinese stalagmite oxygen isotopes are influenced by the upstream moisture source and rainout effect during the moisture transport, which is related to the Asian monsoon, we interpret PC1 as an indicator for monsoon intensity^{31,41,43}. We identify three stages within PC1 which correspond well with the MCA (940–1340 CE), LIA (1340–1840 CE), and CWP (1840–1983 CE), indicating that the large-scale monsoon intensity increased during the MCA, weakened during the LIA, and strengthened again during the CWP. These trends are consistent with monsoon observations and modeling results^{42,44–48}. Interestingly, PC1 follows the effective solar radiation robustly⁴⁵ (Fig. 5a), with a correlation coefficient of 0.42 on a decadal scale ($n = 113$, $P < 0.01$), suggesting that solar irradiance may be the main controlling factor of the Asian monsoon over the last millennium.

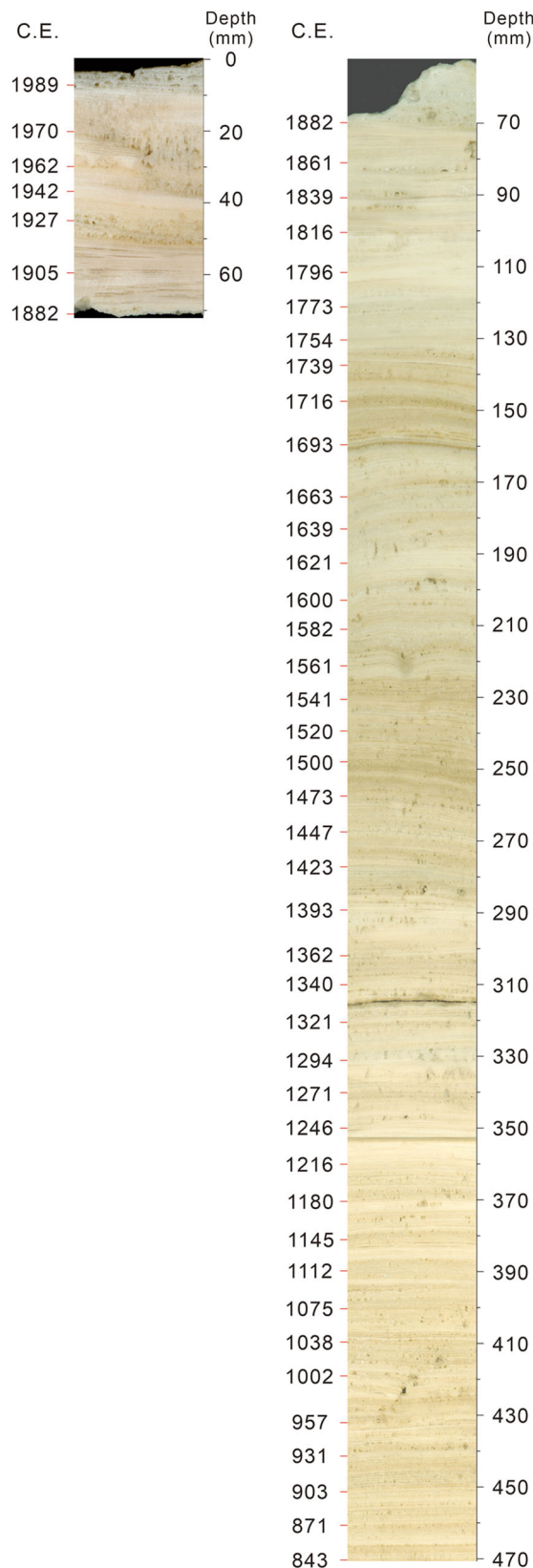


Fig. 2 The sedimentary characteristics and laminations of stalagmite HS4 from Heshang cave in the recent 1150 years. The section consists of two broken parts (the top 7 cm and the rest 40 cm). The numbers along the right and left edges mark the depth and chronology of HS4. Annual-resolved carbonate powder samples were scraped year by year for $\delta^{18}\text{O}$ measurement.

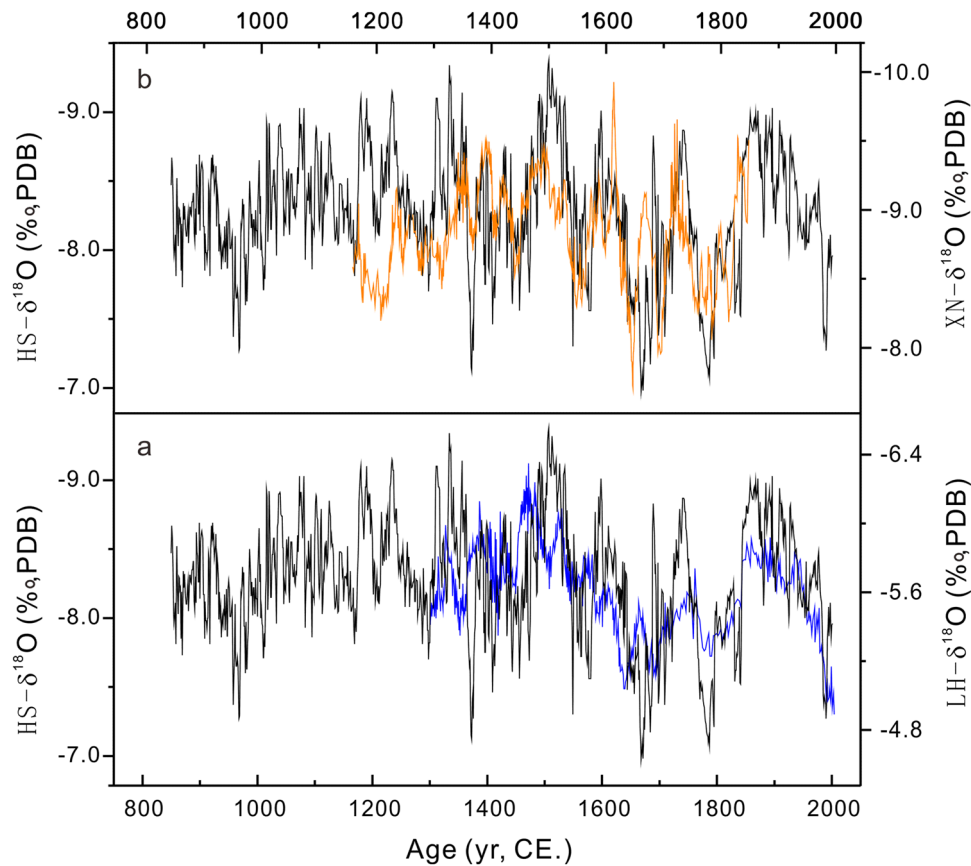


Fig. 3 High-resolved $\delta^{18}\text{O}$ comparisons between HS4 and other stalagmites from Central China. a HS4 in this study and LH from Lianhua cave, Hunan³⁸ (blue curve). **b** HS4 and XN from Xiuniu cave, Hubei³⁹ (orange curve). The HS4 annual $\delta^{18}\text{O}$ record duplicates other high-resolution speleothem records from nearby caves in recent centuries, suggesting the HS4 record could represent the stalagmite $\delta^{18}\text{O}$ variation in Central China.

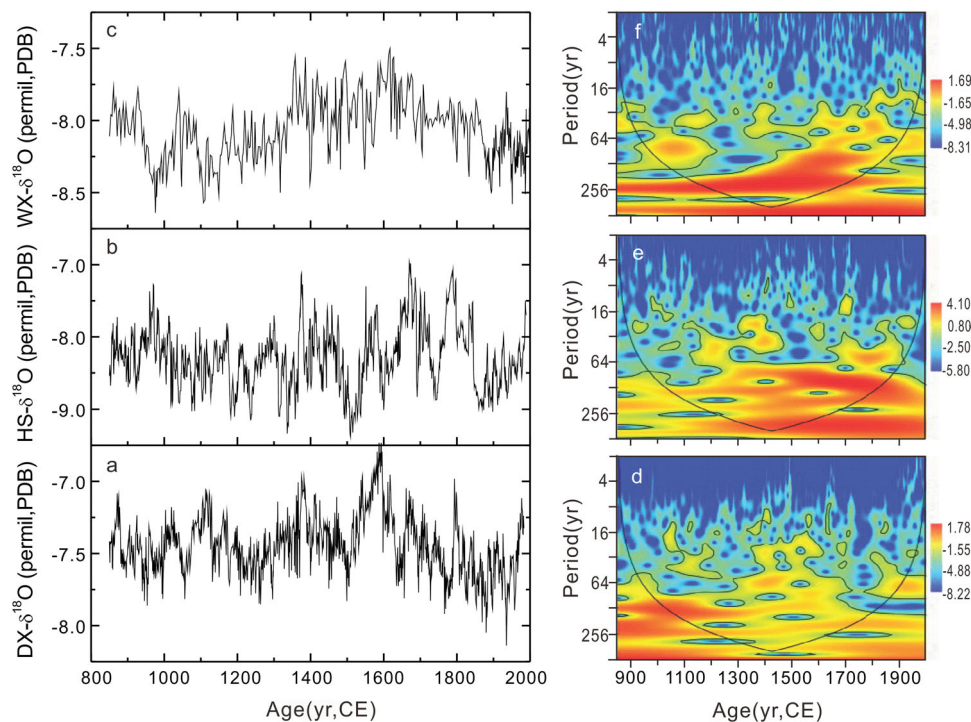


Fig. 4 Comparison of the stalagmite $\delta^{18}\text{O}$ records from DG, HS, and WX cave. The $\delta^{18}\text{O}$ records from DG (a), HS (b), and WX (c), as well as their wavelet analysis (d–f) demonstrate their variations on different time scales with different frequencies and amplitudes, indicating that the contributions of the driving forces to the stalagmite $\delta^{18}\text{O}$ are different from site to site.

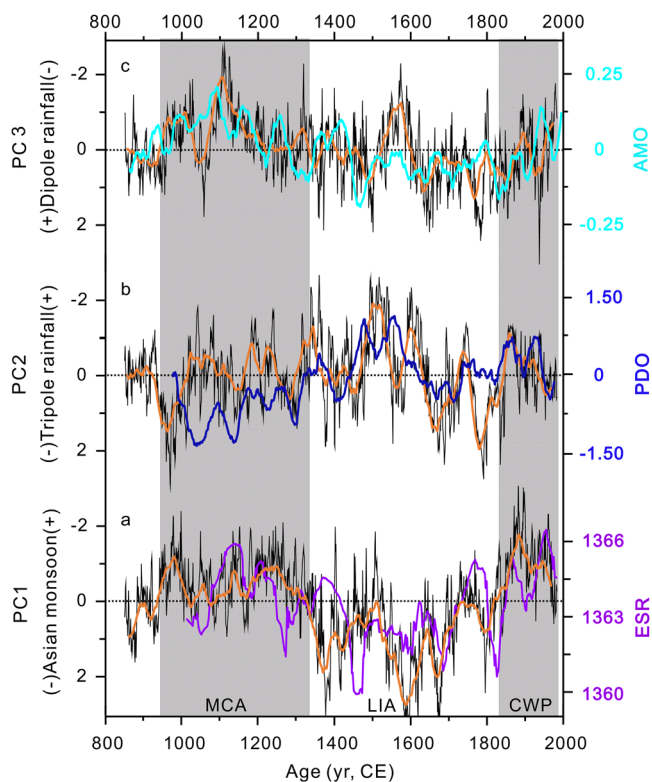


Fig. 5 The principal components analysis of three stalagmite $\delta^{18}\text{O}$ records from the eastern monsoon region of China. The PC1 (a), PC2 (b), and PC3 (c) explain 43.28%, 32.86%, and 24.87% of the variability, representing monsoon, tripole, and dipole rainfall distribution patterns, respectively. The variations of PCs are shown in black thin curves, with their 31-year smoothing average curves shown in orange. Three principal components are consistent with the effective solar radiation⁴⁵ (ESR, purple curve), PDO⁴⁹ (31-year smoothing of the data, dark blue curve), and AMO⁵⁰ (31-year smoothing of data, light blue curve), which means internal climate dynamics persistently impact rainfall distribution in eastern China over the last millennium. The periods of MCA, LIA, and CWP are highlighted in PC1.

PC2 explains 32.86% of the variability, with loadings from DG, HS, and WX $\delta^{18}\text{O}$ records of -0.11 , 0.97 , and -0.22 , respectively. Negative PC2 values imply drier conditions in North and South China, with wetter conditions in Central China, similar to the modern rainfall tripole pattern. In the past 1150 years, the PC2 variation (Fig. 5b) generally corresponds to the 3 stages of the monsoon shown in Fig. 5a. During the LIA, negative PC2 scores imply a tripole rainfall structure ($-/+/-$) following a weak monsoon, which coincides with the modern observation with wet conditions in Central China and drier conditions in South and North China. During medieval and current warm periods (stronger monsoon), the PC2 scores are positive, suggesting wet conditions in South and North China but a dry conditions in Central China ($+/-/+$, an anti-tripole structure). The decadal oscillations of PC2 are consistent with the PDO variation⁴⁹ (Fig. 5b). Linear regression of 11-year average data shows that the PC2-PDO correlation exceeds 95% confidence level ($r = 0.21$, $n = 113$). Positive PDO corresponds to negative PC2, presenting a tripole structure, implying that Pacific dynamics likely dominate the tripole precipitation structure in East China. Our evidence clearly shows that even before industrialization, the tripole pattern of precipitation in East China existed and was likely driven by similar dynamics to the modern.

PC3 explains 24.87% of all variability, and the loadings of DG, HS, and WX $\delta^{18}\text{O}$ records are -0.71 , 0.08 , and 0.70 , respectively. This structure is similar to the observed dipole pattern with opposite precipitation variations between southern and northern China (Fig. 5c). Negative PC3 scores suggest less rainfall in South China but more rainfall in North China (an anti-dipole pattern), which is likely related to the strengthening Asian monsoon during the MCA. Subsequently, during the LIA, the PC3 scores become positive, indicating the rainfall belt moving southward, with a gradual rainfall increase in southern China and a decrease in northern China (dipole pattern). The variation of PC3 is consistent with that of the AMO⁵⁰ (11-year average, $r = 0.25$, $n = 113$, $p < 0.05$), indicating the influence of the North Atlantic on the rainfall in East China (Fig. 5c).

Discussion

The separation of monsoon (PC1) and precipitation signals (PCs 2 and 3) from speleothem $\delta^{18}\text{O}$ allows us to investigate the relationship between tripole and dipole patterns and their link to the monsoon, PDO, and AMO. It is observed that two types of patterns alternate by the influence of the mutual interactions among monsoon, PDO, and AMO on centennial timescales. During the MCA, when a strong monsoon is coupled with a negative PDO and a positive AMO, a dipole pattern of precipitation in East China dominated (PC3 < 0), while the tripole was not significant (PC2 ≈ 0). During the LIA, the precipitation in East China was dominated by a tripole pattern (PC2 < 0) under the conditions of a weak monsoon, a positive PDO, and a negative AMO. In the CWP, the strengthening monsoon, combined with a negative PDO and a positive AMO, initially exhibits a dominant tripole which is gradually replaced by a dipole pattern, similar to the MCA status. This observation coincides with the earlier findings that there are different precipitation patterns during MCA, LIA, and CWP^{16,17}.

On multidecadal timescales, the monsoon, PDO, and AMO also influence the precipitation distribution structure in East China. A bandpass filtering analysis between 20 and 80 years demonstrates that, during a strong monsoon, the main precipitation distributions are shown by a negative tripole pattern (a rainfall increase in South China with a rainfall decrease in Central China and a rainfall increase in North China) and a positive dipole pattern (a rainfall increase in South of China and a rainfall decrease in North China) (Fig. 6). On the other hand, during a weak monsoon, the rainfall distributions are shown as a positive tripole pattern and a negative dipole pattern. The correlations between monsoon (Fig. 6a) and precipitation distribution patterns (Fig. 6b, c) are consistent with modern observations^{2,3,16} and climate modeling^{7,17}. In contrast to the tripole and dipole patterns of rainfall distribution on centennial timescales, and on multi-decadal timescales, the relationships of PC2-PDO and PC3-AMO are unstable. For example, after 1400 CE, the variations of the PDO and PC2 are in-phase, while before 1400 CE, they are anti-phase (Fig. 6b), which suggests that the different climate background states during the MCA and LIA may influence the interaction between PDO and the precipitation distribution pattern in East China. In addition, the interaction between AMO and the precipitation distribution pattern in East China is also unstable (Fig. 6c). During 880–1130, 1310–1500, and 1780–1980 CE, the variations of AMO and PC3 are in-phase, while during 1130–1310 and 1500–1780 CE, they are anti-phase, suggesting that it is not the AMO alone, but the coupling between AMO and PDO that affects the precipitation distribution in East China^{12,51}.

The Western Pacific subtropical high (WPSH) is the bridge between the precipitation patterns in East China and the

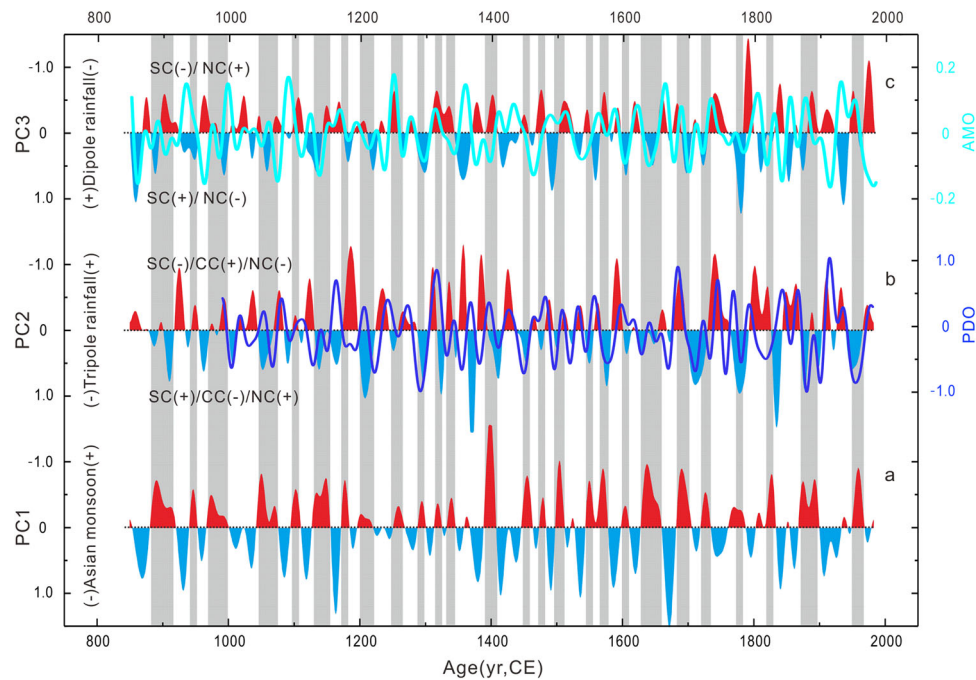


Fig. 6 Interactions between the precipitation distribution pattern in East China and the monsoon with PDO and AMO. All the data are processed by bandpass filtering. **a** The monsoon variation indicated by PC1. **b** The tripole rainfall pattern revealed by PC2 and PDO (in the dark blue). The relationships between them are reversed in 1400 CE. Before 1400 CE, the variations of PC2 and PDO are in-phase, after that, they are anti-phase. **c** The dipole rainfall pattern suggested by PC3 and AMO (in light blue). During 880–1130, 1310–1500, and 1780–1980 CE, the variations of AMO and PC3 are generally in-phase, while during 1130–1310 and 1500–1780 CE, they are anti-phase. On multi-decadal scales, the unstable relationships of PC2–PDO and PC3–AMO suggest that it is the mutual interactions among the monsoon, PDO, and AMO, rather than any individual factor, that influences the precipitation distribution pattern in East China.

monsoon, PDO, and AMO^{7,52–54}. The AMO controls the precipitation distribution in East China with the monsoon and PDO by modifying the middle and high latitude circulation and influencing the intensity and position of the WPSH^{7,54} (Fig. 7). A weak monsoon with positive PDO and negative AMO leads to a southward shift of the WPSH with increasing rainfall in Central China (HS) associated with the Meiyu front, while South China (DG) is covered by the WPSH with decreasing rainfall. At the same time, due to the weakening of the summer monsoon, the moisture transport to North China (WX) is reduced with less rainfall. Thus, the precipitation distribution in East China presents a tripole pattern of ‘-/+/-’ with less rainfall in both South and North China but more rainfall in Central China, a scenario that appeared in LIA (Fig. 5b). On the contrary, during a strong monsoon with a negative PDO and positive AMO, the position of the WPSH moves northward, and Central China (HS) is characterized by high temperatures and less rainfall. The northward shift of the WPSH increased rainfall in South China (DG) and North China (WX) associated with the monsoon trough and Meiyu front^{55,56}. Thus the precipitation distribution in East China presents as an anti-tripole pattern (‘+/-/+’) with increasing rainfall in both South and North China but decreasing rainfall in Central China (Fig. 7b). During the MCA, Asian monsoon further strengthened, and AMO (PDO) was more positive (negative) than the CWP, then WPSH moved further to the northeast, and the monsoon trough leaves off DG site, leading to the precipitation decrease in South China, but increase in North China (WX) and Central China (HS), with a dipole structure shown in Fig. 5c. However, in the past millennium, the monsoon, PDO and AMO were not always coupled (Fig. 6). When they are decoupled, the tripole and the dipole pattern alternate^{12,51}, then the precipitation distribution in East China is

more complex, as we have observed on multi-decadal scales (Fig. 6).

In summary, the monsoon and local precipitation signals are successfully extracted by the principal components analysis on three individual stalagmite $\delta^{18}\text{O}$ records spanning North, Central, and South China, providing important pieces of evidence for understanding the link between local rainfall, the Asian monsoon, and Atlantic and Pacific climate modes. The shared monsoon signal (PC1) recorded at all three locations suggests an influence of solar irradiance on monsoon strength. The reconstructed rainfall records of the last millennium (PCs 2 and 3) suggest that the dipole and tripole structures, which reflect the combined influence of monsoon strength, PDO, and AMO, are persistent over multidecadal to centennial timescales, with potential implications for evaluating climate models and improving future hydroclimate projections.

Materials and methods

Layer identification and chronology. We selected the top section of stalagmite HS4 covering the last 1150 years for this study. The stalagmite is characterized by clear annual growth bands, and each band consists of a light–dark couplet^{23,36,37}. After layer counting, year by year combined with the U–Th dating²³, a precise chronology of stalagmite HS4 from the topmost to 47 cm in depth was established (Fig. 2).

Stable isotopic analysis. On the basis of the above-mentioned stratigraphic identification, we scratched the stalagmite layer by layer for stable isotopic analysis. A total of 1150 samples have been collected for $\delta^{18}\text{O}$ measurements on a Finnigan MAT-253 isotope ratio mass spectrometer with an online, automated carbonate preparation system (GasBench II). The $\delta^{18}\text{O}$ values are reported relative to VPDB (Vienna Pee Dee Belemnite) standard with an external error <0.20‰ (two sigmas).

Principal components analysis. The principal component analysis was carried on by using three stalagmite datasets of oxygen isotope from Dongge cave, Heshang

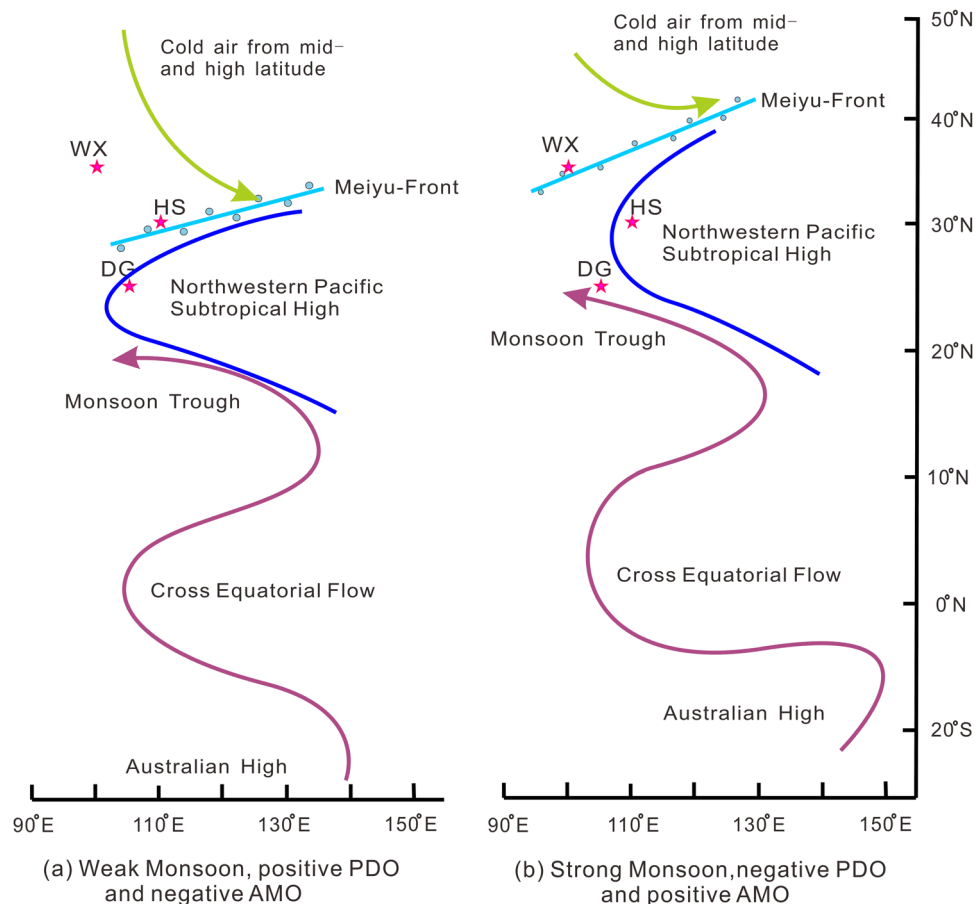


Fig. 7 Schematic diagram of the influence of the Asian monsoon, PDO, and AMO on the precipitation distribution patterns in East China. a A weak monsoon with positive PDO and negative AMO. During this period, the position of the West Pacific subtropical High (WPSH) was southward and Central China (HS) is controlled by Meiyu front with rich rainfall, while South China (DG) and North China (WX) with less rainfall, presenting as a tripole pattern ('-/+/-'). **b** A strong monsoon with negative PDO and positive AMO. During this period, the position of the WPSH was northward, which covered Central China (HS) with less rainfall, while South China (DG) and North China (WX) were controlled by monsoon trough and Meiyu front with rich rainfall, presenting an anti-tropile rainfall pattern ('+/-/+'). This diagram is drawn according to refs. 55,56.

cave, and Wanxiang cave, respectively. We linearly interpolated the WX record to an annual resolution before analysis, to couple the DG and HS datasets, then all of them are annual resolutions. Three principal components are extracted with variances of 43.28%, 32.86%, and 24.87%, respectively.

Data availability

Speleothem $\delta^{18}\text{O}$ data (HS4) and PCA data that support the findings of this study have been deposited in the NOAA Paleoclimatology Data online repository and are available within the Supplementary Data.

Received: 28 July 2022; Accepted: 14 December 2022;

Published online: 22 December 2022

References

- Hsu, H. & Liu, X. Relationship between the Tibetan Plateau heating and East Asian summer monsoon rainfall. *Geophys. Res. Lett.* **30**, 2066 (2003).
- Hsu, H. & Lin, S. Asymmetry of the tripole rainfall pattern during the East Asian Summer. *J. Climate* **20**, 4443–4458 (2007).
- Ding, Y., Wang, Z. & Sun, Y. Inter-decadal variation of the summer precipitation in East China and its association with decreasing Asian summer monsoon. Part I: observed evidences. *Int. J. Climatol.* **28**, 1139–1161 (2008).
- Ding, Y., Sun, Y., Wang, Z., Zhu, Y. & Song, Y. Inter-decadal variation of the summer precipitation in China and its association with decreasing Asian summer monsoon Part II: possible causes. *Int. J. Climatol.* **29**, 1926–1944 (2009).
- Qian, C., Yu, J. & Chen, G. Decadal summer drought frequency in China: the increasing influence of the Atlantic Multi-decadal Oscillation. *Environ. Res. Lett.* **9**, 124004 (2014).
- Wu, X. & Mao, J. Interdecadal variability of early summer monsoon rainfall over South China in association with the Pacific Decadal Oscillation. *Int. J. Climatol.* **37**, 706–721 (2017).
- He, C. et al. Interannual variability of Eastern China Summer Rainfall: the origins of the meridional triple and dipole modes. *Clim. Dynam.* **48**, 683–696 (2017).
- Wang, J. K., Yu, J. & Johnson, K. R. Pacific and Atlantic controls of the relationship between Mainland Southeast Asia and East China interannual precipitation variability. *Clim. Dynam.* **54**, 4279–4292 (2020).
- Sun, B. & Wang, H. Inter-decadal transition of the leading mode of inter-annual variability of summer rainfall in East China and its associated atmospheric water vapor transport. *Clim. Dynam.* **44**, 2703–2722 (2015).
- Ye, H. & Lu, R. Dominant patterns of summer rainfall anomalies in East China during 1951–2006. *Adv. Atmos. Sci.* **29**, 695–704 (2012).
- Sang, Y. et al. Does summer precipitation in China exhibit significant periodicities? *J. Hydrol.* **581**, 124289 (2020).
- Yang, Q. et al. Decadal modulation of precipitation patterns over Eastern China by sea surface temperature anomalies. *J. Climate* **30**, 7017–7033 (2017).
- Qian, C. & Zhou, T. Multidecadal variability of North China aridity and its relationship to PDO during 1900–2010. *J. Climate* **27**, 1210–1222 (2014).
- Linderholm, H. W. et al. Interannual teleconnections between the summer North Atlantic Oscillation and the East Asian summer monsoon. *J. Geophys. Res.* **116**, D13107 (2011).
- Wang, Z., Yang, S., Lau, N. & Duan, A. Teleconnection between summer NAO and East China rainfall variations: a bridge effect of the Tibetan plateau. *J. Climate* **31**, 6433–6444 (2018).

16. Chen, J. et al. Hydroclimatic changes in China and surroundings during the Medieval Climate Anomaly and Little Ice Age: spatial patterns and possible mechanisms. *Quat. Sci. Rev.* **107**, 98–111 (2015).
17. Zhou, X., Zhao, P., Liu, G. & Zhou, T. Characteristics of decadal-centennial-scale changes in East Asian summer monsoon circulation and precipitation during the Medieval Warm Period and Little Ice Age and in the present day. *Chin. Sci. Bull.* **56**, 3003–3011 (2011).
18. Rao, Z. et al. Asynchronous evolution of the isotopic composition and amount of precipitation in north China during the Holocene revealed by a record of compound-specific carbon and hydrogen isotopes of long-chain n-alkanes from an alpine lake. *Earth Planet. Sci. Lett.* **446**, 68–76 (2016).
19. Zhang, H. et al. East Asian hydroclimate modulated by the position of the westerlies during Termination I. *Science* **362**, 580–583 (2018).
20. Cai, Y. et al. Variability of stalagmite-inferred Indian monsoon precipitation over the past 252,000 y. *Proc. Natl Acad. Sci. USA* **112**, 2954–2959 (2015).
21. Cheng, H. et al. Ice age terminations. *Science* **326**, 248–252 (2009).
22. Cheng, H. et al. The Asian monsoon over the past 640,000 years and ice age terminations. *Nature* **534**, 640–646 (2016).
23. Hu, C. et al. Quantification of Holocene Asian monsoon rainfall from spatially separated cave records. *Earth Planet. Sci. Lett.* **266**, 221–232 (2008).
24. Li, Y. et al. Inter-relationship and environmental significance of stalagmite $\delta^{13}\text{C}$ and $\delta^{18}\text{O}$ records from Zhenzhu Cave, north China, over the last 130 ka. *Earth Planet. Sci. Lett.* **536**, 116149 (2020).
25. Wang, Y. et al. Millennial- and orbital-scale changes in the East Asian monsoon over the past 224,000 years. *Nature* **451**, 1090–1093 (2008).
26. Wang, Y. J. et al. A high-resolution absolute-dated late pleistocene monsoon record from Hulu Cave, China. *Science* **294**, 2345–2348 (2001).
27. Yuan, D. et al. Timing, duration, and transitions of the last interglacial Asian monsoon. *Science* **304**, 575–578 (2004).
28. Zhang, P. et al. A test of climate, sun, and culture relationships from an 1810-year Chinese cave record. *Science* **322**, 940–942 (2008).
29. Zhao, K. et al. A high-resolved record of the Asian Summer Monsoon from Dongge Cave, China for the past 1200 years. *Quat. Sci. Rev.* **122**, 250–257 (2015).
30. Liu, Z. et al. Chinese cave records and the East Asia Summer Monsoon. *Quat. Sci. Rev.* **83**, 115–128 (2014).
31. Pausata, F. S. R., Battisti, D. S., Nisancioglu, K. H. & Bitz, C. M. Chinese stalagmite $\delta^{18}\text{O}$ controlled by changes in the Indian monsoon during a simulated Heinrich event. *Nat. Geosci.* **4**, 474–480 (2011).
32. Baker, A. & Bradley, C. Modern stalagmite $\delta^{18}\text{O}$: Instrumental calibration and forward modelling. *Glob. Planet. Change* **71**, 201–206 (2010).
33. Baker, A. et al. Global analysis reveals climatic controls on the oxygen isotope composition of cave drip water. *Nat. Commun.* **10**, 1–7 (2019).
34. Clemens, S. C., Prell, W. L. & Sun, Y. Orbital-scale timing and mechanisms driving Late Pleistocene Indo-Asian summer monsoons: Reinterpreting cave speleothem $\delta^{18}\text{O}$. *Paleoceanography* **25**, A4207 (2010).
35. Editing Commission, The Third National Report on Climate Change of China. *The Third National Report on Climate Change of China (in Chinese)*. (Science Press, Beijing, 2015).
36. Johnson, K., Hu, C., Belshaw, N. & Henderson, G. Seasonal trace-element and stable-isotope variations in a Chinese speleothem: The potential for high-resolution paleomonsoon reconstruction. *Earth Planet. Sci. Lett.* **244**, 394–407 (2006).
37. Liu, Y. et al. Links between the East Asian monsoon and North Atlantic climate during the 8,200 year event. *Nat. Geosci.* **6**, 117–120 (2013).
38. Yin, J. J. et al. Variation in the Asian monsoon intensity and dry-wet condition since the Little Ice Age in central China revealed by an aragonite stalagmite. *Climate Past* **10**, 1305–1335 (2014).
39. Zhao, J. et al. Role of the summer monsoon variability in the collapse of the Ming dynasty: evidences from speleothem records. *Geophys. Res. Lett.* **48**, e2021GL (2021).
40. Tan, M. Circulation effect: response of precipitation $\delta^{18}\text{O}$ to the ENSO cycle in monsoon regions of China. *Clim. Dynam.* **42**, 1067–1077 (2014).
41. Wang, Y., Hu, C., Ruan, J. & Johnson, K. R. East Asian precipitation $\delta^{18}\text{O}$ relationship with various monsoon indices. *J. Geophys. Res.* **125**, e2019JD032282 (2020).
42. Zhang, J., Liang, M., Li, T., Chen, C. & Li, J. Asian-Australian monsoon evolution over the last millennium linked to ENSO in composite stalagmite $\delta^{18}\text{O}$ records. *Quat. Sci. Rev.* **281**, 107420 (2022).
43. Zhou, H. et al. Variation of $\delta^{18}\text{O}$ in precipitation and its response to upstream atmospheric convection and rainout: a case study of Changsha station, south-central China. *Sci. Total Environ.* **659**, 1199–1208 (2019).
44. An, Z. et al. Global monsoon dynamics and climate change. *Annu. Rev. Earth Planet. Sci.* **43**, 29–77 (2015).
45. Liu, J. et al. Centennial Variations of the Global Monsoon Precipitation in the Last Millennium: Results from ECHO-G Model. *J. Climate* **22**, 2356–2371 (2009).
46. Chen, F. et al. Westerlies Asia and monsoonal Asia: spatiotemporal differences in climate change and possible mechanisms on decadal to sub-orbital timescales. *Earth Sci. Rev.* **192**, 337–354 (2019).
47. Shi, F., Li, J. & Wilson, R. J. S. A tree-ring reconstruction of the South Asian summer monsoon index over the past millennium. *Sci. Rep.* **4**, 6739 (2015).
48. Wang, J., Yang, B., Jungqvist, F. C. & Zhao, Y. The relationship between the Atlantic Multidecadal Oscillation and temperature variability in China during the last millennium. *J. Quat. Sci.* **28**, 653–658 (2013).
49. MacDonald, G. M. Variations in the Pacific Decadal Oscillation over the past millennium. *Geophys. Res. Lett.* **32**, L08703 (2005).
50. Wang, J. et al. Internal and external forcing of multidecadal Atlantic climate variability over the past 1,200 years. *Nat. Geosci.* **10**, 512–517 (2017).
51. Zhang, Z., Sun, X. & Yang, X. Understanding the interdecadal variability of East Asian summer monsoon precipitation: joint influence of three oceanic signals. *J. Climate* **31**, 5485–5506 (2018).
52. Dai, G. et al. A modeling study of the triple pattern of east china precipitation over the past 425 ka. *J. Geophys. Res.* **126** (2021).
53. Si, D. & Ding, Y. Oceanic forcings of the interdecadal variability in East Asian summer rainfall. *J. Climate* **29**, 7633–7649 (2016).
54. Weng, H., Lauren, K. M. & Yongkang, X. Multi-scale summer rainfall variability over China and its long-term link to global sea surface temperature variability. *J. Meteorol. Soc. Jpn.* **77**, 845–857 (1999).
55. Ye, D. & Huang, R. *Investigation on Laws and causes of droughts and floods in the yellow river and the Yangtze river valley of China 1 edn. (in Chinese)* (Shandong Science and Technology Press, Jinan, Shangdong, 1996).
56. Tao, S., Zhu, W. & Wei, Z. On the interannual variation of Meiyu. *Chin. J. Atmos. Sci. Special Issue*, 13–21 (1988).

Acknowledgements

We are grateful to Dr. Aliénor Lavergne and three anonymous referees who provided full and insightful comments on an earlier draft of this paper. This work was supported by the National Natural Science Foundation of China (Grant no. 41731177) and the National Key Research and Development Program of China (Grant no. 2016YFA0601100, 2018YFA0605601).

Author contributions

C.-Y.H. designed the research. M.-Y.W. and L.-L.L. contributed to sampling and instrumental measurements of oxygen isotope. All authors contributed to data interpretation and discussion. C.-Y.H. and Y.-H.L. drafted the original paper. The paper was reviewed and edited by S.-C.X. and K.J.

Competing interests

The authors declare no competing interests.

Additional information

Supplementary information The online version contains supplementary material available at <https://doi.org/10.1038/s43247-022-00664-7>.

Correspondence and requests for materials should be addressed to Chaoyong Hu.

Peer review information *Communications Earth & Environment* thanks the anonymous reviewers for their contribution to the peer review of this work. **Primary Handling Editors:** Aliénor Lavergne.

Reprints and permission information is available at <http://www.nature.com/reprints>

Publisher's note Springer Nature remains neutral with regard to jurisdictional claims in published maps and institutional affiliations.



Open Access This article is licensed under a Creative Commons Attribution 4.0 International License, which permits use, sharing, adaptation, distribution and reproduction in any medium or format, as long as you give appropriate credit to the original author(s) and the source, provide a link to the Creative Commons license, and indicate if changes were made. The images or other third party material in this article are included in the article's Creative Commons license, unless indicated otherwise in a credit line to the material. If material is not included in the article's Creative Commons license and your intended use is not permitted by statutory regulation or exceeds the permitted use, you will need to obtain permission directly from the copyright holder. To view a copy of this license, visit <http://creativecommons.org/licenses/by/4.0/>.

© The Author(s) 2022